A Trimodal Framework for Robot-Assisted Vascular Shunt Insertion When a Supervising Surgeon is Local, Remote, or Unavailable

Karthik Dharmarajan[1]*, Will Panitch[1]*, Baiyu Shi[1], Huang Huang[1]
Lawrence Yunliang Chen[1], Thomas Low[2], Danyal Fer[3], Ken Goldberg[1]

Abstract— **Vascular shunt insertion is a common surgical procedure requiring a surgeon-and-surgical-assistant team performed to temporarily restore blood flow to damaged tissues. Robotic assistance for this procedure is challenging due to precision and control uncertainty. The role of the robot in this task depends on the availability of a human surgeon. We propose a trimodal framework for vascular shunt insertion assisted by a dVRK robotic surgical assistant. We consider three scenarios: (1) a surgeon is available locally; (2) a remote surgeon is available via teleoperation; (3) no surgeon is available. In each scenario, the robot operates in a different mode either by teleoperation or automation. For mode (1), a learned visual servoing policy is proposed for vessel grasping. Physical experiments demonstrate a success rate of 70%-100% for mode (1), 100% for mode (2), and 80%-95% for mode (3).**

I. Introduction

Vascular shunt insertion is a surgical procedure that uses a hollow and flexible shunt tube to drain or divert fluid in the human body from one location to another [1]. Vascular shunt surgeries often take place in high-pressure clinical scenarios such as civilian and battlefield settings, where vascular injures are common and a shunt can be utilized to bridge gaps in blood vessels [2, 3]. In most vascular shunt surgeries, a surgical assistant grasps the vessel and the surgeon grasps a third point on the vessel to dilate the vessel and insert the shunt. While precision is critical in this procedure, heavy surgery demand under those scenarios can lead to surgeon fatigue and disruptions. The shortage of surgeons, currently on the rise and projected to be between 15,800 and 30,200 in 2034 [4], led to the closure of more than 100 rural hospitals in the US from January 2013 to February 2020 [5], with 600 more at risk of closure [6]. Utilizing Robotic Surgical Assistants (RSAs) to assist in shunt surgery through either teleoperation or autonomous operation has the potential to mitigate the surgeon shortage, reduce workload, and improve consistency and effectiveness of surgery.

There are 5 key subtasks where robotic assistance may be provided during a vascular shunt procedure:

1) The initial grasp of the blood vessel rim;
2) A secondary grasp of the blood vessel rim, with one grasping point already present;
3) A tertiary grasp of the blood vessel rim, with two grasping points already present;

* equal contribution
[1] The AUTOLab at UC Berkeley (automation@berkeley.edu)
[2] SRI International
[3] UC San Francisco School of Medicine

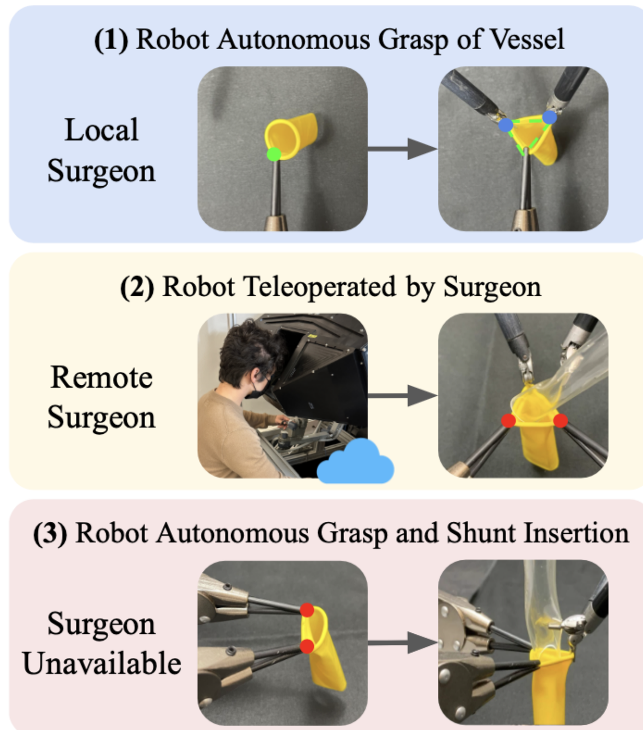

Fig. 1: **Robot Shunt Insertion Trimodal Framework**: Three scenarios are considered: (1) A local surgeon grasps one point (green) of the vessel (yellow balloon) and the robot grasps the other two points (blue) on the vessel automatically. Vessel before (left) and after (right) robot grasping is shown; (2) A remote surgeon (left) teleoperates the robot (right) to grasp the third point and insert the shunt (transparent tube); (3) No surgeon is available. The robot automatically grasps the third point and inserts the shunt. Vessel before (left) and after (right) robot grasping and insertion is shown; In both (2) and (3), the other two points (red) on the vessel are grasped by two passive clamps.

4) Dilation of the blood vessel rim by pulling the third grasp point outward from the rim center;
5) Insertion of the shunt into the dilated vessel.

In previous work, RSAs were teleoperated for phantom vascular shunt insertion operations [7], and in prior work, we proposed a method to automate vascular shunt insertion with a da Vinci Research Kit (dVRK) RSA by dilating a pre-grasped vessel and inserting the shunt, where the success rate varied from 50-80% depending on the size and orientation of the vessel phantom [8].

In this paper, we propose a "trimodal" framework that varies the role of the dVRK for vascular shunt insertion depending on the availability of the surgeon and surgical assistant. Automated blood vessel grasping is challenging

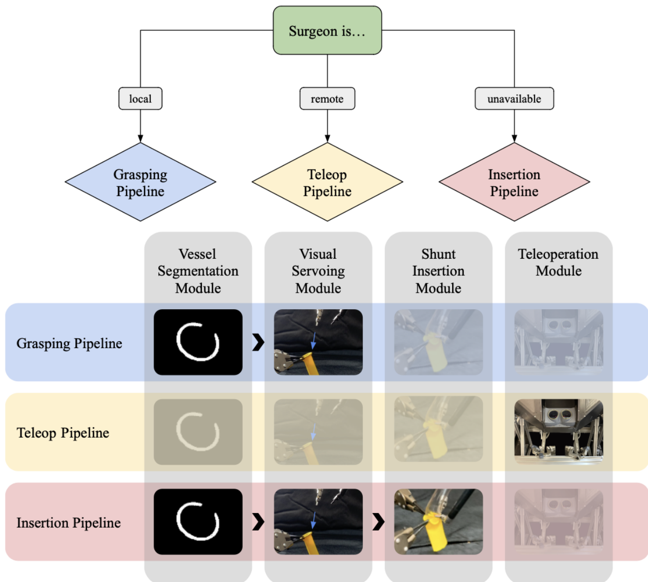

Fig. 2: **Mode Overview**: The system pipeline combines four modules: a *vessel rim state estimation* module, a *visual servoing and grasping* module, a *shunt insertion* module, and a *teleoperation* module. These components are combined into three modes of operation: (1) a grasping pipeline, utilizing the state estimation and the servoing modules, for when a surgeon (but not an assistant) is available locally; (2) a teleop pipeline, utilizing the teleoperation module, for when a surgeon is available remotely and a surgical assistant is available locally; and (3) an insertion pipeline, utilizing the state estimation, servoing, and shunt insertion modules, for when a no surgeon is available, but a surgical assistant is locally available.

due to the deformability of the vessel, self-occlusion of the end effector and vessel rim, and the millimeter-level precision required for grasping. Furthermore, the blood vessel is fragile and an appropriate amount of force must be applied to dilate the vessel without slip or breakage. Hysteresis of the cable-driven dVRK presents extra challenges. We propose a visual servoing policy for autonomous vessel grasping to address those challenges. We conduct physical experiments to evaluate each mode of the trimodal framework.

This paper contributes:

1) A novel trimodal framework for vascular shunt insertion with 4 modules: vessel rim pose estimation, servoing and grasping, shunt insertion, and teleoperation, which adjusts robot roles based on surgeon availability.
2) A visual servoing policy for autonomous vessel grasping using a dVRK from RGB images.
3) Physical experimental results with a human teleoperator and a dVRK for each of the 3 modes that produce a success rate of 100% and an average completion time of between 14.62s and 20.33s for shunt insertion.

II. Related Work

A. Automation in Surgical Robotics

Research in surgical robotics has a long history [9]. Robotic Surgical Assistants (RSAs) are surgical robots designed to help surgeons perform complex surgical procedures such as minimally invasive surgeries, and have been increasingly adopted among high-volume surgeons in the past two decades [10, 11]. They improve surgeon dexterity and visualization [12], and have potential to automate some surgical subtasks to reduce surgeon fatigue [13].

Currently, RSAs are mainly used in hospitals through teleoperation. There are many prior works that study various aspects of improving the surgeon performance and experience of telesurgery, including providing better haptic feedback [14], automating camera movement [15], rating surgeon performance [16], and addressing or compensating for network latency [17, 18].

Recently, many studies have also explored automating surgical subtasks, including tissue manipulation [19], hemostasis [20], debridement [21, 22], suturing and knot tying [23, 24], pattern cutting [25, 26], peg transfer [12, 27, 28], tumor localization and resection [29–31]. Surgical robots, such as the da Vinci Research Kit [32], Raven [33], and SRI International's Taurus Robotic System [34], face a unique challenge for automation as they are driven by cables and can suffer from inaccurate motion and actuation due to backlash hysteresis [35]. Many prior works have proposed methods for calibration [27, 36, 37]. In this work, we consider the vascular shunt insertion task, and we study both the teleoperation scenario and the autonomous robot case.

B. Vascular Shunt Insertion

In military and civilian trauma emergencies, there is often a need for urgent control of hemorrhage and limb ischemia; however, specialized surgeons may not be available or the hospital setting does not allow specialized vascular surgery [38]. In such cases, a surgeon needs to perform damage control by inserting temporary vascular shunts between blood vessels to restore blood flow [2, 3, 39]. The patient will then be transferred to a specialized hospital for a more definitive vascular repair and the shunt will be removed [8, 38]. The development of plastic shunts has proven to be crucial in reducing the amputation rate from vascular injuries in recent battlefields [2, 40].

In a standard (non-robot-assisted) vascular shunt operation [41], a human surgical assistant holds the rim of the blood vessel with two grippers. A surgeon grasps a third point on the rim and dilates the vessel while using another gripper to hold the shunt and insert it into the vessel. This requires both the surgeon and the assistant to be available in person, which may not be the case. In our prior work [8], we explored automating the shunt insertion step of the surgeon with a da Vinci Research Kit and showed that the robot can achieve a success rate between 50% and 80% and an average completion time of between 13.7s and 14.4s, even with tight tolerances and varying vessel orientations up to 30°. In this paper, we consider this and 2 new operational modes and present a robot assistant framework depending on the human operator availability. We perform physical experiments for each of the 3 modes and discuss their pros and cons.

III. Problem Statement

The objective is to fomulate three potential operational scenarios for robot-assisted vascular shunt insertion and propose a paradigm for robotic assistance in each. We provide

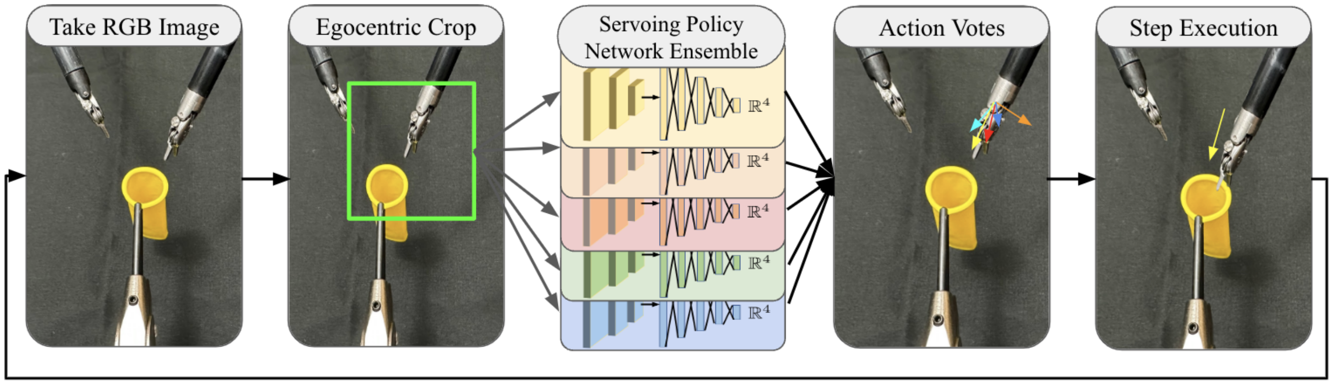

Fig. 3: **Visual Servoing and Grasping Module**: At each step of the visual servoing module, an RGB image is captured by the camera and passed into the pipeline. Using the camera-to-robot transform and the forward kinematics of the robot, this image is cropped to a 180×180 square surrounding the end effector. The crop is passed into an ensemble of convolutional neural networks, whose outputs are an output direction $a \in \{+x, -x, +y, -y\}$. These outputs are collated through voting to determine the direction of motion for this step.

a method for the execution of each paradigm, and evaluate it in terms of success rate and completion time.

A. Assumptions

We assume a blood vessel can be fully opened by three grippers grasping three points as shown in Fig. 1(1) on the right. Initially, we assume that one or two passive grippers hold a vessel phantom, which resembles the role of a surgeon (Fig. 1(1)) or a surgical assistant (Fig. 1(2), Fig. 1(3)) in surgical setting without robots respectively. We assume access to an inclined RGBD camera with known rigid transformations to robot arm coordinate frames. We also assume access to a stereo camera or endoscope that allows a human teleoperator to have a view of the workspace.

We assume that the size of the shunt used in the operation is known, and if the robot is manipulating it, the shunt is held at a known position. We assume the outer radius of the shunt is smaller than the inner radius of the vessel phantom.

B. Objective and Evaluation Metrics

We consider three modes of operation (Fig. 1). For each, we evaluate success and completion time.

Mode (1): Local Surgeon. The surgeon is available locally, and the bimanual surgical robot performs the role of a medical assistant, where it autonomously grasps two points on the vessel phantom given one point grasped by a fixed gripper. A trial is considered successful when both of the robot's grippers are grasping the vessel phantom.

Mode (2): Remote Surgeon. The bimanual surgical robot is teleoperated by a remote surgeon, and a human medical assistant is available locally to grasp the vessel. In particular, we assume two points on the vessel rim are held by fixed grippers, and the teleoperated robot grasps a third point, dilates the vessel phantom, and inserts a shunt. A trial is successful when the shunt rim is fully enclosed within the vessel after both grippers release.

Mode (3): No Surgeon Available. This is an extended version of the case considered by Dharmarajan *et al.* [8] when there is no surgeon available but a human medical assistant is available locally to grasp the vessel, the bimanual surgical robot performs the teleoperated shunt inserter role, where it autonomously grasps the vessel rim on a third point, dilates, and inserts a shunt. A successful trial is defined in the same way as Mode (2).

IV. Method

A. Overview

As illustrated in Fig. 2, the system consists of 4 autonomous components: a vessel phantom rim pose estimator, a grasping and visual servoing module, a shunt insertion procedure, and a teleoperation module. These components can be swapped out and reordered based on the required mode of operation, enabling the system to adapt to different possible on-the-ground situations.

B. Blood Vessel Rim Pose Estimation Module

Before performing any autonomous interaction with the vessel, such as grasping or dilation, we must first detect and characterize the vessel state in space. We utilize a two-step process: segmentation mask generation and curve fitting.

The vessel rim segmentation step takes as input an RGB image of the workspace and converts it to a segmentation mask marking the location of the rim of the vessel. Inspired by Labels from Ultraviolet (LUV) [42], we use ultraviolet paint and a UV–Visible light system to collect 1,500 pairs of UV and Visible light images. We extract masks localized to the vessel rim from the ultraviolet images by applying color thresholding over UV labels and use the image-mask pairs to train an asymmetric U-Net [43, 44]. The architecture consists of a 4-tier contracting path and a 4-tier expansive path to generate the segmentation masks, and we replace the final "up-convolution" level of the expansive path with an upsampling layer to reduce network runtime and parameter count. We use layer depths of 128, 256, 512, and 1,024 channels for both paths and train the model using an Adam optimizer with learning rate $\alpha = 0.001$.

The estimated segmentation mask output is then projected onto the point cloud generated by the RGBD camera to select out the points on the vessel rim in 3D space. We then apply random sample consensus (RANSAC) [45] to estimate

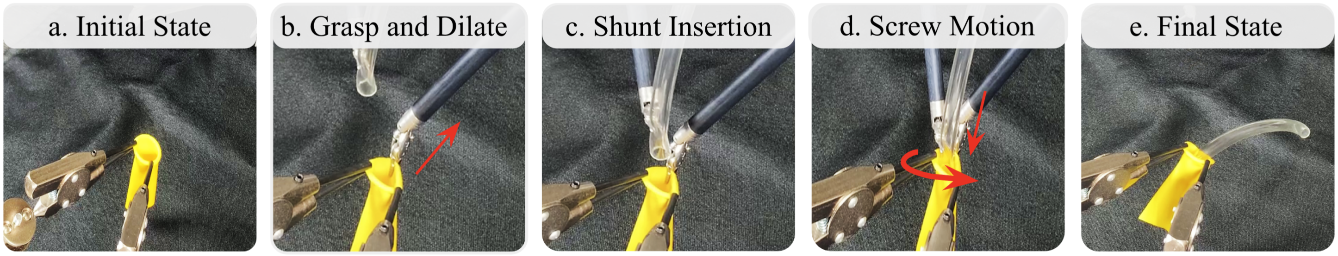

Fig. 4: **Shunt Insertion Module** containing the Chamfer Tilt Shunt Insertion and the Screw Motion. (a) Starting from a surgical assistant grasping two points of the vessel, (b) the robot grasps and dilates a third point on the vessel to open it up. (c) It uses a chamfer tilt insertion motion to insert the shunt and (d) uses a screw motion to screw the shunt inside. (e) After the shunt is fully inserted, the robot releases the grasping of both grippers.

the 3D orientation of the vessel lip represented as a tuple (c_p, c_n, r). The system pipeline uses a RANSAC inlier radius of 1 mm and runs until convergence or for a maximum of 1,000 iterations to minimize the stochastic error between the 3D depth images and masking pipeline.

C. Servoing and Grasping Module

The servoing and grasping module uses the sensed 3D location and orientation of the vessel rim and attempts to actuate the robot to an intended grasping point on its rim. An open-loop policy calibrated using the method outlined in Seita *et al.* [22] is used to actuate to the intended 3D location for grasping. Once the gripper is within 2 mm horizontally of its target, a visual servoing policy takes over.

The visual servoing module, shown in Fig. 3, utilizes two policies, π_{right} and π_{left}, to take corrective actions for the right and left arms respectively. Each policy takes in a 180×180 RGB image cropped around their respective grippers and outputs an action direction $a \in \{+x, -x, +y, -y\}$. The image cropping forces the policy to learn about the relative positions of the grippers and the vessel, reducing the overfitting against specific features from other parts of the workspace. Furthermore, the actions are motions with magnitudes between 0.2 mm and 0.8 mm along the x- or y-axis in the robot coordinate frames.

The policies are represented as a neural network ensemble consisting of 5 lightweight convolutional neural networks, each consisting of 3 convolutional layers and 5 fully connected layers. To train the policies, offline human demonstrations of 150 trajectories consisting of 15–30 actions were collected using a keyboard teleoperation interface, resulting in 4,303 image-action pairs. The networks are trained using a cross-entropy classification loss.

During execution time, we take the majority vote among the five ensemble networks as the direction for the robot to move. The magnitude of the first action is 0.8 mm. If consecutive actions are in opposite directions, the magnitude of subsequent actions are halved. When the action magnitude goes below a threshold of 0.2 mm, the servoing terminates. The policies do not need to explicitly learn a stopping action, as the decaying action magnitudes from consecutively moving in opposite directions converges.

Since there are two arms, each with a similar task that does not depend on the other, grasping can be executed either sequentially or concurrently. In sequential execution, one arm first servos and grasps the vessel rim, and then the second arm follows. In concurrent execution, both arms can be run concurrently to reduce the time it takes to perform bimanual vessel grasping. In the concurrent version of servoing, the policies π_{right} and π_{left} each retrieve a corresponding cropped image from the camera, compute the desired actions, and execute the desired actions on separate threads. Once both grippers are finished servoing, they move downward concurrently and grasp the vessel. Once a successful grasp is performed, the grippers simultaneously move outward from the center to tension the vessel rim. We report experiments with both sequential and concurrent movements.

D. Shunt Insertion Module

After the dilation step, the rim of the vessel phantom is enlarged, as shown in Fig. 4(b) indicated by the red arrow. The gripper and any fixed points used to tension the vessel now become obstacles that must be avoided during the insertion of the shunt, reducing the range of motion available. The vessel phantom also cannot be overly stretched due to the possibility of slip or tearing, further decreasing the size of the target. To overcome the challenges associated with these low tolerances, the insertion module makes use of the chamfer tilt–screw motion insertion combination proposed in Dharmarajan *et al.* [8] to insert tightly fitting shunts.

1) Chamfer Tilt Insertion: The robot approaches the insertion from above with the shunt held at an angle, presenting the end of the shunt corner-first for insertion. The end effector is first actuated to a point slightly above the vessel phantom rim, then moves downward, inserting the leading edge of the tilted shunt below the lip of the vessel. Once the shunt is partially seated below the rim, the end effector rotates to straighten the shunt, while at the same time, the arm dilating the vessel moves upward and inward to improve quality of the fit, as in Fig. 4(c).

2) Screw Motion: In some cases, after the chamfer tilt insertion motion is completed, a portion of the shunt remains outside of the rim of the vessel. In this case, this motion alone is not sufficient to ensure that the shunt remains in place after both grippers release their grips. To increase the chance that the entire shunt is situated within the rim of the vessel, the robot executes a screw motion, which is a counterclockwise rotation combined with a concurrent downward translation,

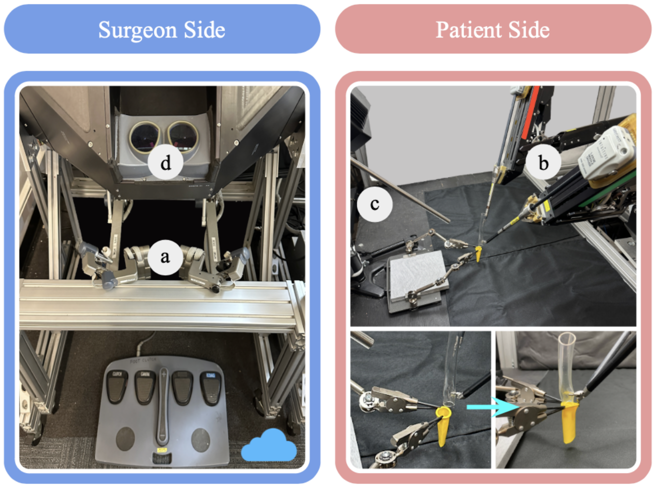

Fig. 5: **Teleoperation Setup**: The remote teleoperation setup includes: the two master tool manipulators (labeled "(a)"), which pass the motion commands from the remote surgeon to the the two patient side manipulators (labeled "(b)"), and an endoscope (labeled "(c)"), which captures binocular vision information and transmits it to the surgeon's console (labeled "(d)"). The goal of the teleoperation mode is to insert the shunt into the vessel phantom, as illustrated in the bottom right.

as shown by the red arrow in Fig. 4(d). This motion helps bring any portion of the shunt that was previously above or outside the rim inside. After the completion of this motion, both grippers release their grasps and retract to a home position away from the insertion site.

E. Teleoperation Module

In the teleoperation mode, a human teleoperator uses the dVRK controller with two tool manipulators and foot pedals to control both grippers of the surgical robot. One gripper first grasps and dilates the vessel, and then the other gripper, already holding a shunt, inserts the shunt into the vessel.

V. Experiments

Servoing	**Execution Model**	**Success Rate**	**Avg trial time** *(s)*	**Failure Modes** (O)	(T)
N	Sequential	95%	13.2 ± 0.39	0	1
	Concurrent	65%	7.7 ± 0.37	7	0
Y	Sequential	70%	17.4 ± 0.73	6	0
	Concurrent	100%	10.4 ± 0.42	0	0

TABLE I: **Mode 1: Bimanual Vessel Grasping Results:** Success rate and mean trial time for bimanual grasping with and without servoing, along with executing both arms' motions sequentially and concurrently. We track two failure modes: (O) One arm grasping failure and (T) Two arm grasping failure.

A. Experimental Setup

We perform experiments using the da Vinci Research Kit (dVRK) surgical robot with two cable-driven patient-side manipulator (PSM) arms [46]. For autonomous roles, the robot captures RGBD images at a 1920x1200 resolution with 30 fps using an inclined Zivid One Plus S camera. The teleoperation interface consists of foot pedals, two master tool manipulators (MTMs), and a stereo viewer, as shown in Fig. 5. There are two mounted arms to hold the vessel if the robot is performing shunt insertion, and only one can be used when the robot is grasping two points.

Mode	**Diameter** *(mm)*	**Success Rate**	**Avg trial time** *(s)*	**Failure Modes** (D)	(S)
2	8	100%	13.6 ± 0.58	0	0
	14	100%	20.3 ± 7.7	0	0
3	8	95%	14.5 ± 0.58	0	1
	14	80%	14.4 ± 0.54	0	4

TABLE II: **Modes 2 (Teleoperation) and 3 (Surgeon Unavailable): Shunt Insertion Results:** Success rate and mean trial time for shunt insertion with varying shunt outer diameters and insertion modes. We track two failure modes: (D) dilation failure and (S) shunt insertion failure.

The vessel phantom used for experiments is the tube-top of a yellow latex balloon with an inner diameter of 15 mm and a rim thickness of 1.5 mm. The shunts used are two clear vinyl tubes with outer diameters of 8 mm and 14 mm.

B. Bimanual Vessel Grasping Metrics and Failure Modes

As described in Section III-B, we consider a bimanual grasping trial successful if both of the robot grippers are grasping the vessel phantom. For this mode, we classify the failures into one of the following:

1) One-arm grasping failure (O): Either the left or right arm attempts to grasp the vessel phantom, but misses. When the gripper is closed, there is no part of the vessel phantom inside it.

2) Two-arm grasping failure (T): Both the left and right arms attempt to grasp the vessel phantom, but both miss.

C. Bimanual Vessel Grasping Results

As shown in Table I, we perform 20 trials of bimanual vessel grasping, where the dVRK autonomously grasps two points on the vessel rim without servoing, with servoing, each with their sequential and concurrent variants. For each set of 20 trials, the center of the vessel is placed at 4 different points for 5 trials each. The 4 points form a square with a side length of 2.54 cm.

For bimanual grasping without servoing, we observe that the success rate declines from 95% to 65% when the execution model changes from sequential to concurrent, and there are 7 one-arm grasping failures (O) and 1 two-arm grasping failure (T) respectively. For bimanual grasping with servoing, we observe that the success rate increases from 70% to 100% when the execution model changes from sequential to concurrent, and there are 6 one-arm grasping failures (O) and 0 failures respectively.

For sequential execution, all of the one-arm failures (O) occurred on the second arm after the first arm had grasped the vessel. When the first arm is grasping the vessel, the vessel tilts at an angle that is out of distribution from the human demonstrations, resulting in incorrect servoing actions. This does not occur in the concurrent execution case where both arms servo concurrently because only after both are done servoing do they move downward and grasp the vessel.

We observe that on average, the duration of the concurrent execution of bimanual vessel grasping is less by 5.5 s in the no servoing case, and 7.0 s in the servoing case.

D. Shunt Insertion Metrics and Failure Modes

We consider a shunt insertion trial, both for teleoperation as well as autonomous insertion, a success if one arm is able to dilate the vessel and the other arm is able to insert a shunt, such that the rim of the shunt is fully enclosed when both grippers release. The elapsed time of each trial as well as the success or failure of that trial is noted. Failures can fall into two categories:

1) Dilation failure (D): The robot, commanded with instructions from a teleoperator or through the autonomous pipeline, either attempts to grasp the vessel phantom and fails, or successfully grasps it but fails to dilate the vessel phantom rim outward.

2) Shunt insertion failure (S): After both grippers release the vessel phantom and the shunt, if even a small portion of the shunt's rim is outside of the vessel phantom, it is considered a failure.

E. Teleoperation Results

For 20 trials of inserting the 8mm and 14mm outer diameter shunts, one co-author (W. Panitch) served as the human teleoperator after 15 hours of experience. We report the results in Table II. We observe that the human teleoperator has a 100% success rate for inserting both the 8mm and 14mm outer diameter shunts. The average trial time increased from 14.6 s to 20.3 s when the shunt outer diameter increased from 8 mm to 14 mm.

F. Autonomous Shunt Insertion Results

We perform 20 trials of autonomous shunt insertion when a surgeon is unavailable with both the 8mm and 14mm outer diameter shunts, and report the results in Table II.

We observe that the autonomous shunt insertion pipeline achieves a success rate of 95% with the 8 mm outer diameter shunt and 80% with the 14 mm outer diameter shunt. There were no dilation failures, but there were 1 and 4 shunt insertion failures respectively. The average time of each trial is 14.5 s and 14.4 s respectively.

VI. Limitations

The methods proposed and settings considered have a number of limitations when compared to the clinical setting.

The vessel phantoms and shunts considered are 1.5–2.0× larger than their analogues in clinical settings, and are constructed from materials that may not perfectly reflect the appearance or behavior of in-vivo vascular tissues or shunts. Additional work is required to apply these techniques to any in-vivo setting.

The teleoperation mode assumes continuous access to a high-speed, low-latency network connection for both the operating surgeon and the patient-side robot. This is often unavailable in the disaster or battlefield scenarios where vascular shunt insertion is in high demand.

During experiments, the local surgical assistant is represented by a pair of fixed grippers. However, a human assistant is not necessarily stationary, which suggests a potential to help or hinder the autonomous components—for example, by maneuvering the vessel rim to make it easier to localize and grasp, or disrupting the visual servoing system with unintended motion. We hope that future work will consider the potential to apply techniques from multi-agent planning or human-robot interaction literature to this setting.

While the state of the vessel is monitored visually by the perception system, force feedback is not available to the dVRK. This makes it difficult to consider the stress applied to the vessel during tensioning, which could lead to tears in the vascular tissue. In addition, the shunt is not actively tracked, and the system is not robust to unknown orientations of the shunt in the robot grippers.

VII. Discussion

In this paper, we propose a trimodal framework for vascular shunt insertion and provide experimental results demonstrating its efficacy, even in the presence of tight tolerances and cable slippage. To improve the accuracy of our model under these adversarial conditions, we present a novel visual servoing module for grasping in the automated vascular shunt insertion problem. Our results show that the proposed method achieves a high success rate across all three modes of operation, even without a surgeon present. While human-driven methods such as teleoperation or in-person surgery continue to have the highest success rates, our results suggest that autonomy-assisted surgery is a promising option for patients in situations where face-to-face surgical care is inaccessible.

Acknowledgments

This research was performed at the AUTOLAB at UC Berkeley in affiliation with the Berkeley AI Research (BAIR) Lab and the CITRIS "People and Robots" (CPAR) Initiative. This work is supported in part by the Technology & Advanced Telemedicine Research Center (TATRC) project W81XWH-19-C-0096 under a medical Telerobotic Operative Network (TRON) project led by SRI International and donations from Intuitive Surgical. The da Vinci Research Kit is supported by the National Science Foundation, via the National Robotics Initiative (NRI) [46]. We also thank Michael Yip at the University of California, San Diego and Sanjay Krishnan at the University of Chicago for collaborating on this project.

References

[1] J. Cannon, *Shunt procedure*, Feb. 2018.

[2] A. Subramanian, G. Vercruysse, C. Dente, A. Wyrzykowski, E. King, and D. V. Feliciano, "A decade's experience with temporary intravascular shunts at a civilian level i trauma center," *Journal of Trauma and Acute Care Surgery*, vol. 65, no. 2, pp. 316–326, 2008.

[3] T. E. Rasmussen, W. D. Clouse, D. H. Jenkins, M. A. Peck, J. L. Eliason, and D. L. Smith, "The use of temporary vascular shunts as a damage control adjunct in the management of wartime vascular injury," *Journal of Trauma and Acute Care Surgery*, vol. 61, no. 1, pp. 8–15, 2006.

[4] T. Dall, R. Reynolds, R. Chakrabarti, D. Chylak, K. Jones, and W. Iacobucci, *The complexities of physician supply and demand: Projections from 2019 to 2034*, Jun. 2021.

[5] G. A. Office, *Rural hospital closures: Affected residents had reduced access to health care services*, Dec. 2020.

[6] CHQPR, *Rural hospitals at risk of closing*, Oct. 2022.

[7] P. Garcia, J. Rosen, C. Kapoor, M. Noakes, G. Elbert, M. Treat, T. Ganous, M. Hanson, J. Manak, C. Hasser, *et al.*, "Trauma pod: A semi-automated telerobotic surgical system," *The International Journal of Medical Robotics and Computer Assisted Surgery*, vol. 5, no. 2, pp. 136–146, 2009.

[8] K. Dharmarajan, W. Panitch, M. Jiang, K. Srinivas, B. Shi, Y. Avigal, H. Huang, T. Low, D. Fer, and K. Goldberg, "Automating vascular shunt insertion with the dvrk surgical robot," 2022.

[9] G. Moustris, S. Hiridis, K. Deliparaschos, and K. Konstantinidis, in *Evolution of Autonomous and Semi-Autonomous Robotic Surgical Systems: A Review of the Literature*, vol. 7, International Journal of Medical Robotics and Computer Assisted Surgery, 2011.

[10] B. Chughtai, D. Scherr, J. D. Pizzo, M. Herman, C. Barbieri, J. Mao, A. Isaacs, R. Lee, A. E. Te, S. A. Kaplan, P. Schlegel, and A. Sedrakyan, in *National Trends and Cost of Minimally Invasive Surgery in Urology*, vol. 2, Urology Practice, 2015.

[11] S. L. Chang, A. S. Kibel, J. D. Brooks, and B. I. Chung, in *The Impact of Robotic Surgery on the Surgical Management of Prostate Cancer in the USA*, vol. 115, BJU International, 2014.

[12] M. Hwang, D. Seita, B. Thananjeyan, J. Ichnowski, S. Paradis, D. Fer, T. Low, and K. Goldberg, "Applying depth-sensing to automated surgical manipulation with a da vinci robot," in *2020 International Symposium on Medical Robotics (ISMR)*, IEEE, 2020, pp. 22–29.

[13] M. Yip and N. Das, in *Robot Autonomy for Surgery*, The Encyclopedia of Medical Robotics, 2017.

[14] A. Abiri, J. Pensa, A. Tao, J. Ma, Y.-Y. Juo, S. J. Askari, J. Bisley, J. Rosen, E. P. Dutson, and W. S. Grundfest, "Multi-modal haptic feedback for grip force reduction in robotic surgery," *Scientific reports*, vol. 9, no. 1, pp. 1–10, 2019.

[15] I. Rivas-Blanco, C. J. Perez-del-Pulgar, C. López-Casado, E. Bauzano, and V. F. Muñoz, "Transferring know-how for an autonomous camera robotic assistant," *Electronics*, vol. 8, no. 2, p. 224, 2019.

[16] J. D. Brown, C. E. O'Brien, S. C. Leung, K. R. Dumon, D. I. Lee, and K. J. Kuchenbecker, "Using contact forces and robot arm accelerations to automatically rate surgeon skill at peg transfer," *IEEE Transactions on Biomedical Engineering*, vol. 64, no. 9, pp. 2263–2275, 2016.

[17] J. Marescaux, J. Leroy, F. Rubino, M. Smith, M. Vix, M. Simone, and D. Mutter, "Transcontinental robot-assisted remote telesurgery: Feasibility and potential applications," *Annals of surgery*, vol. 235, no. 4, p. 487, 2002.

[18] G. Gonzalez, M. Agarwal, M. V. Balakuntala, M. M. Rahman, U. Kaur, R. M. Voyles, V. Aggarwal, Y. Xue, and J. Wachs, "Deserts: Delay-tolerant semi-autonomous robot teleoperation for surgery," in *2021 IEEE International Conference on Robotics and Automation (ICRA)*, IEEE, 2021, pp. 12 693–12 700.

[19] C. Shin, P. W. Ferguson, S. A. Pedram, J. Ma, E. P. Dutson, and J. Rosen, "Autonomous tissue manipulation via surgical robot using learning based model predictive control," in *2019 International Conference on Robotics and Automation (ICRA)*, IEEE, 2019, pp. 3875–3881.

[20] F. Richter, S. Shen, F. Liu, J. Huang, E. K. Funk, R. K. Orosco, and M. C. Yip, "Autonomous robotic suction to clear the surgical field for hemostasis using image-based blood flow detection," *IEEE Robotics and Automation Letters*, vol. 6, no. 2, pp. 1383–1390, 2021.

[21] B. Kehoe, G. Kahn, J. Mahler, J. Kim, A. Lee, A. Lee, K. Nakagawa, S. Patil, W. D. Boyd, P. Abbeel, *et al.*, "Autonomous multilateral debridement with the raven surgical robot," in *2014 IEEE International Conference on Robotics and Automation (ICRA)*, IEEE, 2014, pp. 1432–1439.

[22] D. Seita, S. Krishnan, R. Fox, S. McKinley, J. Canny, and K. Goldberg, "Fast and reliable autonomous surgical debridement with cable-driven robots using a two-phase calibration procedure," in *2018 IEEE International Conference on Robotics and Automation (ICRA)*, IEEE, 2018, pp. 6651–6658.

[23] S. Sen, A. Garg, D. V. Gealy, S. McKinley, Y. Jen, and K. Goldberg, in *Automating Multiple-Throw Multilateral Surgical Suturing with a Mechanical Needle Guide and Sequential Convex Optimization*, IEEE International Conference on Robotics and Automation (ICRA), 2016.

[24] D.-L. Chow and W. Newman, "Improved knot-tying methods for autonomous robot surgery," in *2013 IEEE International Conference on Automation Science and Engineering (CASE)*, IEEE, 2013, pp. 461–465.

[25] A. Murali, S. Sen, B. Kehoe, A. Garg, S. McFarland, S. Patil, W. D. Boyd, S. Lim, P. Abbeel, and K. Goldberg, "Learning by observation for surgical subtasks: Multilateral cutting of 3d viscoelastic and 2d orthotropic tissue phantoms," in *2015 IEEE International Conference on Robotics and Automation (ICRA)*, IEEE, 2015, pp. 1202–1209.

[26] B. Thananjeyan, A. Garg, S. Krishnan, C. Chen, L. Miller, and K. Goldberg, "Multilateral surgical pattern cutting in 2d orthotropic gauze with deep reinforcement learning policies for tensioning," in *2017 IEEE International Conference on Robotics and Automation (ICRA)*, IEEE, 2017, pp. 2371–2378.

[27] M. Hwang, B. Thananjeyan, S. Paradis, D. Seita, J. Ichnowski, D. Fer, T. Low, and K. Goldberg, "Efficiently calibrating cable-driven surgical robots with rgbd fiducial sensing and recurrent neural networks," *IEEE Robotics and Automation Letters*, vol. 5, no. 4, pp. 5937–5944, 2020.

[28] S. Paradis, M. Hwang, B. Thananjeyan, J. Ichnowski, D. Seita, D. Fer, T. Low, J. E. Gonzalez, and K. Goldberg, "Intermittent visual servoing: Efficiently learning policies robust to instrument changes for high-precision surgical manipulation," in *2021 IEEE International Conference on Robotics and Automation (ICRA)*, IEEE, 2021, pp. 7166–7173.

[29] A. Garg, S. Sen, R. Kapadia, Y. Jen, S. McKinley, L. Miller, and K. Goldberg, "Tumor localization using automated palpation with gaussian process adaptive sampling," in *2016 IEEE International Conference on Automation Science and Engineering (CASE)*, IEEE, 2016, pp. 194–200.

[30] S. McKinley, A. Garg, S. Sen, D. V. Gealy, J. P. McKinley, Y. Jen, M. Guo, D. Boyd, and K. Goldberg, "An interchangeable surgical instrument system with application to supervised automation of multilateral tumor resection," in *2016 IEEE International Conference on Automation Science and Engineering (CASE)*, IEEE, 2016, pp. 821–826.

[31] M. Hwang, B. Thananjeyan, D. Seita, J. Ichnowski, S. Paradis, D. Fer, T. Low, and K. Goldberg, "Superhuman surgical peg transfer using depth-sensing and deep recurrent neural networks," *arXiv preprint arXiv:2012.12844*, 2020.

[32] G. H. Ballantyne and F. Moll, "The da vinci telerobotic surgical system: The virtual operative field and telepresence surgery," *Surgical Clinics*, vol. 83, no. 6, pp. 1293–1304, 2003.

[33] B. Hannaford, J. Rosen, D. W. Friedman, H. King, P. Roan, L. Cheng, D. Glozman, J. Ma, S. N. Kosari, and L. White, "Raven-ii: An open platform for surgical robotics research," *IEEE Transactions on Biomedical Engineering*, vol. 60, no. 4, pp. 954–959, 2012.

[34] *Taurus: This small robot is reaching new heights and solving once-thought impossible challenges*, `https://medium.com/dish/taurus-this-small-robot-is-reaching-new-heights-and-solving-once-thought-impossible-challenges-e858fdbbb4ab`.

[35] H. Kim, M. Hwang, J. Kim, J. M. You, C.-S. Lim, and D.-S. Kwon, in *Effect of Backlash Hysteresis of Surgical Tool Bending Joints on Task Performance in Teleoperated Flexible Endoscopic Robot*, vol. 16, The International Journal of Medical Robotics and Computer Assisted Surgery, 2020.

[36] M. Haghighipanah, M. Miyasaka, Y. Li, and B. Hannaford, "Unscented kalman filter and 3d vision to improve cable driven surgical robot joint angle estimation," in *2016 IEEE international conference on robotics and automation (ICRA)*, IEEE, 2016, pp. 4135–4142.

[37] H. Peng, X. Yang, Y.-H. Su, and B. Hannaford, "Real-time data driven precision estimator for raven-ii surgical robot end effector position," in *2020 IEEE International Conference on Robotics and Automation (ICRA)*, IEEE, 2020, pp. 350–356.

[38] E. Hornez, G. Boddaert, U. Ngabou, S. Aguir, Y. Baudoin, N. Mocellin, and S. Bonnet, "Temporary vascular shunt for damage control of extremity vascular injury: A toolbox for trauma surgeons," *Journal of visceral surgery*, vol. 152, no. 6, pp. 363–368, 2015.

[39] A. N. Abou Ali, K. M. Salem, L. H. Alarcon, G. Bauza, E. Pikoulis, R. A. Chaer, and E. D. Avgerinos, "Vascular shunts in civilian trauma," *Frontiers in surgery*, vol. 4, p. 39, 2017.

[40] M. E. DeBakey and F. A. Simeone, "Battle injuries of the arteries in world war ii: An analysis of 2,471 cases," *Annals of surgery*, vol. 123, no. 4, p. 534, 1946.

[41] E. J. Voiglio, V. Dubuisson, D. Massalou, Y. Baudoin, J. Caillot, C. Létoublon, and C. Arvieux, "Abbreviated laparotomy or damage control laparotomy: Why, when and how to do it?" *Journal of visceral surgery*, vol. 153 4 Suppl, pp. 13–24, 2016.

[42] B. Thananjeyan, J. Kerr, H. Huang, J. E. Gonzalez, and K. Goldberg, "All you need is luv: Unsupervised collection of labeled images using invisible uv fluorescent indicators," *arXiv preprint arXiv:2203.04566*, 2022.

[43] O. Ronneberger, P. Fischer, and T. Brox, "U-net: Convolutional networks for biomedical image segmentation," in *International Conference on Medical image computing and computer-assisted intervention*, Springer, 2015, pp. 234–241.

[44] S. Rosas Gonzalez, T. Birgui-Sekou, M. Hidane, and I. Zemmoura, "Asymmetric ensemble of asymmetric u-net models for brain tumor segmentation with uncertainty estimation," *Frontiers in Neurology*, vol. 12, p. 609 646, Sep. 2021.

[45] M. A. Fischler and R. C. Bolles, "Random sample consensus: A paradigm for model fitting with applications to image analysis and automated cartography," *Communications of the ACM*, vol. 24, no. 6, pp. 381–395, 1981.

[46] P. Kazanzides, Z. Chen, A. Deguet, G. Fischer, R. Taylor, and S. DiMaio, in *An Open-Source Research Kit for the da Vinci Surgical System*, IEEE International Conference on Robotics and Automation (ICRA), 2014.